Carbohydrate Polymers 347 (2025) 122771

Contents lists available at ScienceDirect

Carbohydrate Polymers

journal homepage: www.elsevier.com/locate/carbpol

Exploring the effects of cellulose sources on silver reduction and the bacterial removal of nanocellulose-based hydrogel beads

Diego Gomez-Maldonado [a,1], Brieanne R. Dickson [a], Gabriel Au [a], Michael J. Bortner [b,c], Mi Li [d], Eduardo Espinosa [e], Alejandro Rodriguez [e], Brendan Higgins [f], Maria S. Peresin [a,*]

[a] Sustainable Bio-based Materials Laboratory, Forest Products Development Center, College of Forestry, Wildlife and Environment, Auburn University. 602 Duncan Dr, Auburn, AL 36849, United States
[b] Macromolecules Innovation Institute, Virginia Tech, Blacksburg, VA 24061, United States
[c] Department of Chemical Engineering, Virginia Tech, Blacksburg, VA 24061, United States
[d] Center for Renewable Carbon, School of Natural Resources, The University of Tennessee, Knoxville, TN 37996, United States
[e] BioPrEn Group (RNM 940), Área de Ingeniería Química, Instituto Químico para la Energía y el Medioambiente, Facultad de Ciencias, Universidad de Córdoba, Córdoba 14014, Spain
[f] Biosystems Engineering, College of Engineering, Auburn University, 520 Devall Dr, Auburn, AL 36849, United States

ARTICLE INFO

Keywords:
Silver nanoparticles
Cellulose nanofibrils
Regenerated cellulose
Soybean hulls
Oat straws
Softwood
E. coli

ABSTRACT

With water access challenged, there is a need to develop efficient and sustainable alternatives for water purification. Here, cellulose nanofibrils (CNFs) isolated from three source materials (softwood, soybean hulls and oat straw) were compared for the generation of hydrogels beads, and compared as support and reducing agent for silver nanoparticles formation. The silver-functionalized hydrogel beads (Ag-CNFs) were characterized, and the surface energy and specific surface area were evaluated. Antimicrobial testing was conducted to assess the efficacy of the Ag-CNFs against *E. coli*. The results showed that the Ag-CNFs had a higher specific surface area and lower surface energy compared with unmodified CNFs. Softwood-based Ag-CNFs exhibited the highest silver content and specific surface area, while the soybean hull based showed the highest hydrophobic character. The silver-functionalized soybean hull beads (Ag-sbCNF) showed the highest efficacy in reducing the growth of bacteria. Overall, this study highlights the potential of silver-functionalized CNFs hydrogel beads as a promising environmentally friendly and sustainable material for water filtration and disinfection. The findings also suggest that lower surface energy of the Ag-CNFs play an important role in their antimicrobial effect on tested water by enabling shorter retention, providing useful insights into the design of future water filtration materials.

1. Introduction

The pursuit for bio-based, low cost, and effective water remediation materials has risen in parallel to environmental awareness and challenges. One of these challenges relates to new trends on invasive wildlife species movement and relocation -such as wild pigs- that impact the quality of water sources such as lakes and rivers used for human consumption and recreation (Bolds et al., 2021; McDonough et al., 2022). This is particularly harmful in rural and isolated areas worldwide (Barth et al., 2018; Bolds et al., 2022), where concentrations of *E. coli* range between 10^3 and 10^9 CFU/mL, concentrations higher than those considered pathogenic for humans (Ishii & Sadowsky, 2008). Therefore, there is a need to develop sustainable, equitable, and locally sourced antimicrobial filtration systems that can be used as point-of-use in low income and remote areas.

One recognized short contact strategy to eliminate bacteria and other coliforms from water sources is the use of silver nanoparticles (AgNPs) (Liao et al., 2019). These nanoparticles are of interest because of their effectiveness and wide variety of green production methods, which include plant and animal extractives that can be used as a reduction and stabilizing agents (Vishwanath & Negi, 2021). Using green and local reagents in the design is congruent with the international sustainable goals. However, AgNPs are colloidally stable when free, which would mean that they will wash off when in contact with flowing water. To alleviate this, immobilization in 3D structures is needed for their use in efficient water remediation strategies. Polymeric substrates stand out as

* Corresponding author.
E-mail address: soledad.peresin@auburn.edu (M.S. Peresin).
[1] Current address: Department of Chemical Engineering, Northeastern University, Boston, MA 02115, United States.

https://doi.org/10.1016/j.carbpol.2024.122771
Received 13 February 2024; Received in revised form 13 September 2024; Accepted 17 September 2024
Available online 22 September 2024

potential materials due to their low density, processability, and the ability to be shaped. Using biopolymers, and most specifically natural polymers, would allow silver nanoparticle antimicrobials to reduce their carbon footprint while improving biodegradability after their end of the functional lifetime.

Among the various natural polymers available, cellulose present the advantages of wide abundance and the possibility of being obtained from different raw materials (Klemm et al., 2005). Moreover, cellulose nanomaterials (CNMs) can be isolated with varying surface charge and intrinsic properties depending on the source and isolation process (Foster et al., 2018; Iglesias et al., 2020, 2021). This variability among CNMs can be exploited to assert various degrees of modification when grafting polymers or growing nanoparticles on their high surface area (Drogat et al., 2011; Feng et al., 2014; Roy et al., 2009; Stinson-Bagby et al., 2019; Valencia et al., 2020; Wohlhauser et al., 2018). Furthermore, some modified cellulosic materials have proven to be advantageous in water remediation strategies as well as in the elimination of bacteria from water sources (Carpenter et al., 2015; Lin et al., 2015; Olivera et al., 2016).

Hence, silver nanoparticles-cellulose composites are an attractive system to explore as antibacterial materials. There is a wide variety of processes in which they can be generated, tending to present extended active lifetimes when compared to organic antimicrobials, and having relative nontoxicity to eukaryotic cells (Fiorati et al., 2020; Xu et al., 2018). However, ecotoxicity may still become a problem if silver ions are liberated too fast (Fiorati et al., 2020). To address this issue, design strategies where the nanoparticles are grown *in situ*, ion liberation is slow, and other phenomena help control contact time and ion release are promising alternatives to overcome these issues (Karlsson et al., 2019; Wu et al., 2014). Likewise, the antibacterial materials need a shape that facilitates their packing into filtration systems, maximizing surface area and allowing short residence times for the treated water.

Due to their high-water retention and efficient packing shape (Gomez-Maldonado, Ponce, & Peresin, 2022), regenerated cellulose hydrogel beads could serve as a suitable substrate material for further modification and functionalization towards antimicrobial systems. Particularly their solid content – and therefore surface area – can be tuned in the starting cellulose solution, while avoiding crosslinking or other chemical modification of exposed moieties (Gericke et al., 2013; Wang et al., 2016). Traditionally, these hydrogel beads have been made from pure dissolving pulp; however, recently we demonstrated that these beads can be produced using nanocellulose fibril as a starting material (Gomez-Maldonado, Ponce, & Peresin, 2022). This provides multiple advantages, such as the capability of using agri-residues as sources that include residual polymeric fractions such as residual lignin, pectin, and other hemicelluloses and their respective functionalities. Thus, it is worth exploring the difference in performance that the different source materials will give in applications such as the generation of scaffold hydrogels for silver reduction in antimicrobial systems.

In this work, a comparison of the formability of regenerated cellulose hydrogel beads starting from three sources of CNFs (softwood pulp, and the agri-residues: soybean hulls and oat straw) was evaluated, aiming to demonstrate the effect of the source material on the AgNP formation and consequent antibacterial capacity. With the working hypotheses i) the source's physicochemical properties would impact the surface area and surface energy of the hydrogel beads; ii) higher initial surface charge would increase the reducing capacity, generating more AgNPs on the regenerated hydrogel beads; and iii) higher AgNP content would have stronger antimicrobial effects, enabling shorter retention times. A graphical flow of the study is presented in Fig. 1.

2. Experimental

2.1. Materials and reagents

Production of the softwood cellulose nanofibrils (swCNF, 2.07 wt%, pH 6.1) and bleached soybean hull nanofibrils (sbCNF, 2.11 wt% pH 4.9) was done at the Sustainable Bio-Based Materials Lab at Auburn University (Auburn, AL, USA) by mechanical fibrillation. Briefly, Southern Bleached Softwood Kraft pulp with a standard composition of <1 % lignin, 97.1 % cellulose, and 2.0 % hemicellulose (Małachowska et al., 2020) was washed for 30 min in water at pH 3, lowered with 1 M HCl, followed by rinse with DI water until pH was between 4.5 and 5; then the pulp was transferred to a 0.001 M $NaHCO_3$ bath with a pH 9 for 30 min. After rinsing with DI water until constant conductivity, a 2 wt% suspension was processed in a Masuko Super Mass Colloider (MKZA-10-15 J, Masuko Sangyo Co., Ltd., Japan) with 20 passes (Gomez-Maldonado et al., 2021). Meanwhile, sbCNFs were isolated from soybean hulls with a composition of 11.9 % Klason lignin, 63.6 % holocellulose, and 9.1 % pectin (Hernandez et al., 2022). As described, the soybean hulls were placed in a 0.1 N HCl suspension for 1 h at 90 °C to extract the pectin, after filtration, sodium chlorite was added at a 1:25 fiber to liquor ratio for 1 h at 75 °C and the bleaching was stopped with rinses with DI water until pH was 7. The pulp was then washed as described for the Southern Bleached Softwood Kraft pulp and a 2 wt% suspension was mechanically fibrillated with 12 passes in the Masuko Super Mass Colloider (Hernandez et al., 2022). Bleached oat straw nanofibrils (osCNF, 1.58 wt % pH 5.9) were produced at the Universidad de Córdoba (Córdoba, Spain) as described in Espinosa et al. (Espinosa et al., 2017). In brief, a pulp with 5.3 % lignin, 14.8 % hemicelluloses, and 76.4 % cellulose was pretreated with an Novozym 476 enzyme cocktail using a 0.83 % enzyme dosage based (o.d.m) in 1.5 L of buffer water pH 5, with a ratio of 50 g pulp/L at 50 °C for 3 h, the hydrolysis was stopped by heating the suspension to 80 °C for 15 min. Then the pulp was washed with DI water changes until no changes in pH were measured; afterwards, the pulp was diluted to a 1 wt% suspension that was passed 10 times through a pressure homogenizer PANDA 2000 (Gea Niro Soavi, Italy).

Urea and nitric acid were procured from VWR (Randor, PA, USA); while NaOH pearls (97 % purity) and Agar were bought from Alfa Aesar (Ward Hill, MA, USA). Sodium nitrate was obtained from Acros Organics

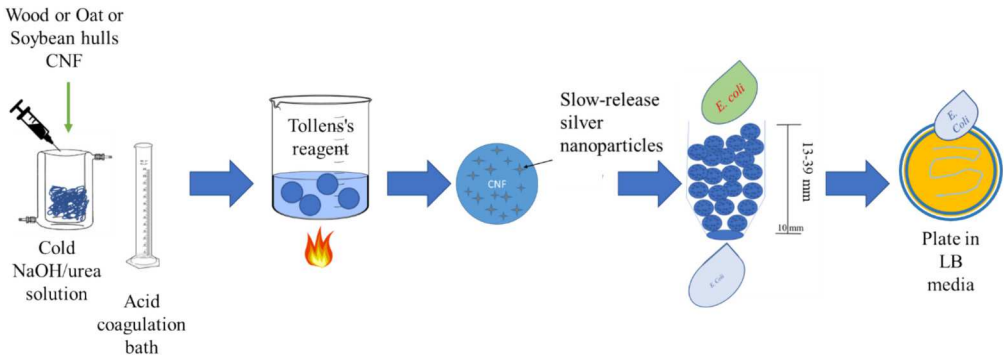

Fig. 1. Schematic of the experimental flow in this article.

(Waltham, MA, USA). Ammonium hydroxide (18–30 % solution) was produced by Millipore Sigma (San Luis, MO, USA). Polydiallyldimethylammonium chloride (pDADMAC) and potassium polyvinyl sulfate (PVSK) were purchased from BTG Americas (Norcross, GA, USA). 1× phosphate buffer saline (PBS), Luria broth (LB), and Luria Agar media were all prepared according to protocols described in Cold Spring Harbor Protocols (2006, 2006, 2009). Ultrapure water was purified from distilled water by a ThermoScientific Barnstead Nanopure system (18.2 mΩ cm). Unless specified, all weights indicated in this manuscript are oven dry basis.

2.2. Bacterial inoculum

E. coli (ATCC 25922) was transferred from glycerol stock into LB in a 50 mL Falcon centrifuge tube and grown overnight at 37 °C and 7.38 rcf in an orbital incubator. The culture was then centrifuged for 5 min in 2050 rcf to pellet out the *E. coli*. LB was removed from the tube and the pellet was resuspended in 1× PBS. Alternatively, for subsequent executions, an extra agar plate was swabbed with the inoculum before testing and incubated with the test and control plates. *E. coli* was then directly swabbed from the extra plate into 2–3 mL of PBS to create a suspension. For both methods, optical density (OD_{600}) was measured by spectrophotometer (Thermoscientific Genesys 50) and adjusted to 0.5 with PBS to create the testing inoculum.

2.3. Cellulose hydrogel beads fabrication

The beads were generated as previously described in Gomez-Maldonado et al. (Gomez-Maldonado, Ponce, & Peresin, 2022). Briefly, a 2 wt% nanocellulose suspension was mixed with urea, sodium hydroxide, and water was added to achieve a final concentration of 12 % urea - 7 % NaOH at −10 °C. Once a homogeneous solution was formed, the solution was added dropwise to a volumetric cylinder containing 2 M nitric acid through a syringe with a 21G 100 (0.8192 mm outer diameter) needle. Once the cellulose was regenerated, the water was exchanged for fresh ultrapure water until a neutral pH was achieved.

2.4. Preparation of Tollens' reagent and in situ silver nanoparticle synthesis

The silver nanoparticle synthesis method was adapted from one described previously in the literature (Wu et al., 2014). Briefly, 10 mL of 0.1 M Tollens' reagent was prepared by dissolving 0.1698 g of silver nitrate and 50 μL of sodium hydroxide in ultrapure water. Next, 860 μL of ammonium hydroxide was added to the solution, activating the solution while changing its color from transparent to brown. The solution was then diluted to a 0.03 M concentration in a 15 mL solution containing 3 cm^3 of nanocellulose hydrogel beads, 6.5 mL of ultrapure water, and 4.5 mL of the silver ammonia solution. The beads were left to impregnate with silver ions in an orbital rotator for 15 h, followed by the reduction of the silver by immersing them into a water bath at 80 °C for 10 min. The beads were immediately rinsed out with ultrapure water until no changes in pH or conductivity were measurable, assuring that the silver content measured was not from residual salts.

2.5. Characterization techniques

2.5.1. Charge density

The amount of charged moieties in the CNMs was evaluated by inverse polymer titration. The protocol was adapted from Espinosa et al. (2016) with the different nanocellulose suspensions being measured 6 times and the results averaged. Briefly, CNFs suspensions at 0.04 wt% were prepared, 15 mL of the suspension were then mixed with 25 mL of pDADMAC. The mixture was centrifugated at 2050 rcf for 15 min, then 10 mL of the solution were placed into a Laboratory Charge Analyzer Chemtrac LCA-1, (Norcross, GA, USA). Titration with PSVK was done until the current value was 0, the PSVK volume consumed was used with the following equation (Eq. 1).

$$Charge\ density = \frac{([pDADMAC]^{*}V_{p-DADMAC}) - ([PVSK]^{*}V_{PVSK})}{W_{dry\ sample}} \quad (1)$$

where [pDADMAC] was the concentration of the cationic polymer used and $V_{p\text{-}DADMAC}$ is the volume added. [PVSK] was the concentration of the anionic polymer, and V_{PVSK} the volume used for titration. Lastly, $W_{dry\ sample}$ was the weight of the solid content of nanocellulose titrated.

2.5.2. Dynamic light scattering (DLS)

The hydrodynamic radius and zeta potential were investigated by triplicate measurements of 0.1 wt% suspensions in a Litesizer from Anton-Paar (Gratz, Austria). For all samples, triplicate measurements were done using the Omega cuvettes and the default settings for solvent, approximation model, and reference material.

2.5.3. Fourier transformed infrared spectroscopy with attenuated total reflectance (FTIR-ATR)

Chemical characterization of the CNMs and formed hydrogels was done to determine the present functional groups. Samples were analyzed in a PerkinElmer Spotlight 400 FT-IR Imaging System (Waltham, MA, US) with a diamond/ZnSe crystal ATR accessory using a resolution of 4 cm^{-1} and 64 scans. All data was processed with Spectrum 6 Spectroscopy Software (PerkinElmer, Massachusetts, USA). Normalization to the lower band (1150 cm^{-1}) was done for all the spectra and automatic base line correction was run to improve comparison capacity of the resulting bands.

2.5.4. X-ray diffraction (XRD)

To assess the presence of the AgNPs and changes to the hydrogel bead cellulose, freeze-dried samples were grounded and analyzed in a RIGAKU Smartlab SE model equipped with Cu Kα irradiation (λ = 1.541 Å) at 40 kV and 50 mA. Measurements were done at a scan speed of 0.01 s/step, from 5° to 80°, using a 0.5 slit and step speed of 20°/min.

2.5.5. Thermogravimetric analysis (TGA)

Thermal behavior and degradation points of the nanocellulose hydrogel beads were evaluated. For this, samples were measured in a TGA Q5000IR from Waters TA Instruments (New Castle, DE, USA). The samples were heated from room temperature to 600 °C under air at a rate of 10 °C/min.

2.5.6. Scanning electron microscopy (SEM)

To compare the nanocellulose hydrogel beads morphology and architecture, samples were fractured with the aid of liquid nitrogen then placed onto aluminum stubs and sputtered with gold for 95 s in a Q150R ES sputter coating device from Electron Micros- copy Sciences (Hatfield, PA, USA). Images were recorded at 20 kW and working distances between 7 and 10 mm in a Zeiss Evo 50VP scanning electron microscope (Oberkochen, Germany).

2.5.7. Inverse gas chromatography (iGC)

The surface area and energy profiles of the freeze-dried beads were obtained in an iGC Surface Energy Analyzer (SMS, Alperton, UK) and the data were analyzed using both standard and advanced SEA Analysis Software. The freeze-dried samples were packed into individual silanized glass columns and the experiment was conducted as described elsewhere (Gomez-Maldonado, Reynolds, et al., 2022).

2.5.8. Inductively coupled plasma with optical emission spectrometry (ICP-OES)

For the quantification of the silver content in the nanocellulose hydrogel beads, samples were prepared according to the EPA (US Environmental Protection Agency, 1996). Briefly, dried samples were

placed in 2.5 mL of ultrapure water to obtain a 5 mg/mL suspension. Then, 12.5 mL of nitric acid (70 %) were added, and the tube was sonicated in a heating bath for 1.5 h. Lastly, 1 mL of the digested solution was placed in 39 mL of ultrapure water to obtain a 0.02 % hydrolyzed stock for testing. Prior to testing, the samples were evaluated using DLS to confirm that no AgNPs were present. The samples were measured in a Spectro ATCOS II Multi View ICP-OES detected at 328 nm with the detection limit of 0.001 mg/L. Each measurement presented is an average of 3 integrations.

2.6. Antimicrobial testing

To test antimicrobial properties, *E. coli* contaminated water at varying bacteria concentration was flowed through the filtration packing column, a 3 mL syringe barrel, filled to 13 cm, 26 cm, and 39 cm height, with either the silver decorated or control nanocellulose hydrogel beads. A schematic of the testing design is presented in Fig. 2. To obtain the bacteria, an inoculum was prepared in LB or from plates and adjusted to 0.5 OD_{600} with PBS. Afterwards, serial dilutions of the inoculum were performed to obtain dilutions at 10^{-8}, 10^{-7}, and 10^{-6} (approx. 0–2 CFU/mL, 5–20 CFU/mL, and 200–600 CFU/mL, respectively). For each packing column, 3 mL were applied by triplicate, with the last flow-through milliliter collected in a 1.5 mL microcentrifuge tube for each condition, resulting in 1, 2, and 3 s residency times depending on the column height. 100 μL of the flow-through bacteria suspension was collected and plated onto sterile Luria agar plates using conventional spread plate technique. 100 μL of the diluted bacterial inoculums were also spread plated for controls. The agar plates were incubated overnight at 37 °C and colonies were counted after incubation. Log reduction was calculated (Eq. 2) to determine the antimicrobial efficacy, where A is the initial (neg control) colonies and B is the colony numbers after antimicrobial treatment (flow-through).

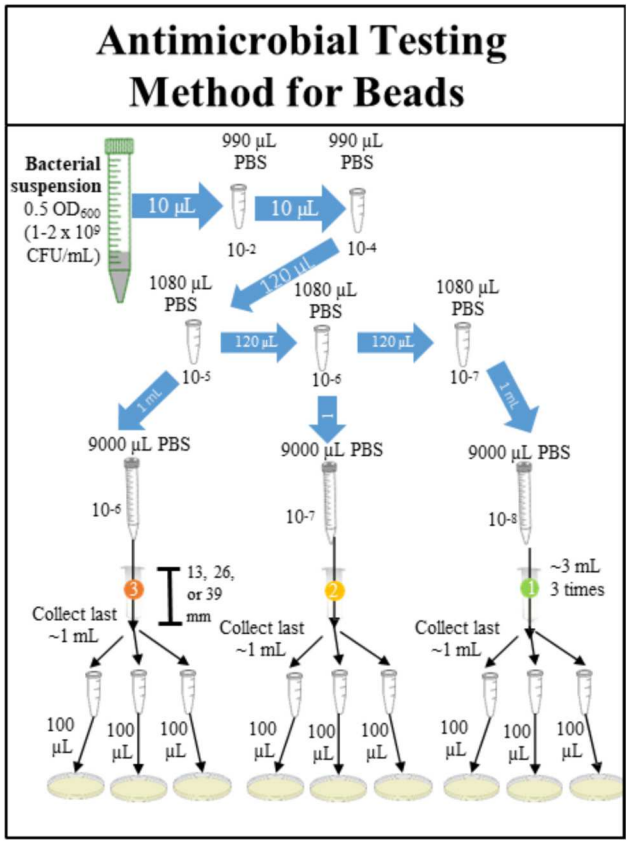

Fig. 2. Schematic of the antimicrobial testing design.

$$log\ \text{reduction} = log_{10}\left(\frac{A}{B}\right) \quad (2)$$

2.7. Statistical analysis

To examine the impact of the antimicrobial capabilities of different materials, at different filter heights with different bacteria concentration on the reduction of bacterial growth a multifactor one-way ANOVA was conducted. The reduction of bacterial growth was log-transformed to approach normality (Sokal & Rohlf, 1987). The model was fitted using source material (3 levels), presence of nanoparticles (2 levels), filter heights (3 levels), and the CFU initial concentration (3 levels) as fixed variables. Interactions were included in the model to assess the combined influence of the fixed variables. When a significance difference between groups was identified ($P < 0.05$), a *post hoc* Tuckey HDS was performed to determine which groups were different. All analyses were carried out in the statistical software R (R Core Team, 2023).

3. Results

3.1. Nanocellulose suspension properties

To address the first hypothesis "the source material's physicochemical properties would impact the surface area and surface energy of the hydrogel beads", the hydrodynamic radius, zeta potential, and polyelectrolyte consumption -which relates to surface charge density- were measured for the starting materials and the results are presented in Table 1. Further characterization of these CNFs can also be found in previous reports, specifically the softwood (swCNF) (Gomez-Maldonado et al., 2021), soybean hull (sbCNF) (Iglesias et al., 2021), and oat straw (osCNF) (Espinosa et al., 2017).

The swCNF was obtained from Kraft pulp and bleached as they are industrially done for paper and tissue formation. These presented the highest residual carboxyl group content and smallest hydrodynamic radius. The size distribution could likely be linked to the highly branched structures seen in the atomic force microscopy (AFM) images (Gomez-Maldonado et al., 2021).

The second highest charge density was for the sbCNF, which also had the higher zeta potential, this is linked to colloidal stability (Iglesias et al., 2023). These CNFs had the intermediate hydrodynamic radius, however, had the lower polydispersity which is most likely benefited by the shorted fibers observed with AFM (Iglesias et al., 2021).

The osCNF showed a higher hydrodynamic radius but a lowest value for zeta potential and charge density. The lower zeta potential and long fibers would consequently tend to aggregate to form compact coiled fibrils in the suspensions (Redlinger-Pohn et al., 2017).

The difference in these nanocelluloses from different sources gives some indication of the main properties that could affect subsequent structure assembly and their properties. For example, degree of polymerization, which varies between sources as well as by the processing done, can impact the mechanical properties after regeneration (De Silva & Byrne, 2017). Here, this was not measured, but the particle size can give hints as it was observed in our previous work that decreasing dimensions allowed for the use of nanocellulose in the formation of hydrogel beads (Gomez-Maldonado, Ponce, & Peresin, 2022). This also allowed for the integration of other polysaccharides as well as other

Table 1
Charge density and DLS data from the raw materials.

	Polyelectrolyte consumption [μeq/g]	Hydrodynamic radius [nm]	Zeta potential [mV]
swCNF	−186 ± 24	223 ± 120	−20.2 ± 0.8
sbCNF	−129 ± 22	318 ± 0.3	−27.0 ± 0.7
osCNF	−54.7 ± 11	372 ± 54	−14.7 ± 0.2

polymeric biomass fractions like lignin (results not published).

The presence of functionality on the surface is of interest as it is expected to impact the surface charge and therefore the reducing capacity of the cellulose to serve as seeding points for the growth of silver nanoparticles (Wu et al., 2014). Thus, understanding the physicochemical characteristics of the initial CNFs is of high importance for the valorization of these agri-residues in the development of new effective products like the antimicrobial hydrogels explored here.

3.2. Nanocellulose hydrogel beads assembly and silver nanoparticle synthesis

The three CNFs sources used in this study were capable of dissolving and regenerating under the same conditions to form hydrogel beads. Using CNFs as starting material allowed the use of agri-residues as source material rather than the traditional pretreated wood dissolving pulp, using only mechanical treatment to decrease the degree of polymerization instead of chemical (Trygg & Fardim, 2011) or enzymatical (Qi et al., 2008). This as the dissolution of the cellulose in the cold NaOH/urea solution is improved by the maximization of surface area, allowing for more hydrogen bonding between cellulose chains and the urea (Jiang et al., 2014), even if residues of other biopolymers are still present in the cellulose suspensions.

A successful reduction of the silver ions added with the Tollens' reagent into Ag nanoparticles on the hydrogel cellulose fibers was first observed by the color change consequent to the plasmon resonance of the formed nanoparticles (Yang et al., 2016). The swCNF beads exhibited the highest color change, turning into a deep brown color like those observed in colloidal silver (Drogat et al., 2011), followed by a yellow tint to the osCNF beads, and almost no coloration on the wet sbCNF beads. However, all silver-containing beads showed a brown color in the dry powders upon freeze-drying. These differences confirmed the first hypothesis regarding the effect of the initial source in the properties of the nanocellulose hydrogel beads. Further characterization was done to assess which properties changed and to confirm the relationship between surface charge and silver content.

FTIR spectra was done as a qualitative analysis of the chemical footprint of the materials (Fig. 3). In general, subtle differences between the cellulose hydrogel beads were observed, especially in the areas of the bands around 3000–2700 cm^{-1} corresponding to the C—H stretching (Fig. 3b) and the C═O region around 1800–1500 cm^{-1} (Fig. 3c). To better see these differences, the first derivative of the spectra (Fig. S1) was obtained to see the changes as peaks and valleys corresponding to the changes in slopes.

For the cellulose hydrogel beads before AgNP formation, differences are observable between the bands at 2870–2850 cm^{-1} and particularly for the osCNF, a peak in the derivative (Fig. S1b) can be seen at 1760 cm^{-1}. These differences suggest the presence of residual hemicelluloses and pectin as they were in the fibrils before regeneration (Fan et al., 2012).

Once the nanoparticles were formed, the main differences can be seen in the C—H stretching bands. There was an increase in the intensity of the bands at 2925 and 2855 cm^{-1}, as well as the appearance of a shoulder at 2917 and 2850 cm^{-1}. These bands are most likely linked to the oxidation of the cellulose and ring opening as a result of the Tollens' reagent which formed new aldehyde groups (Wu et al., 2014).

XRD spectra were collected to better identify changes in the material with the growth of the AgNPs (Fig. 4). A broad peak at 21° was observed for all the hydrogel beads, which is characteristic of cellulose II allomorph (Garcia et al., 2021). The apparent low concentration of AgNPs

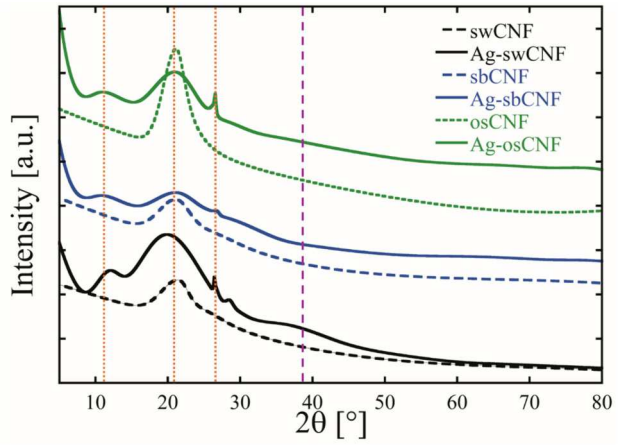

Fig. 4. XRD spectra of (a) the beads before and after AgNP formation. The orange short dashed lines indicate the peak attributed to the cellulose II allomorph and the purple long dashed line to the peak at 39° linked to silver nanoparticles.

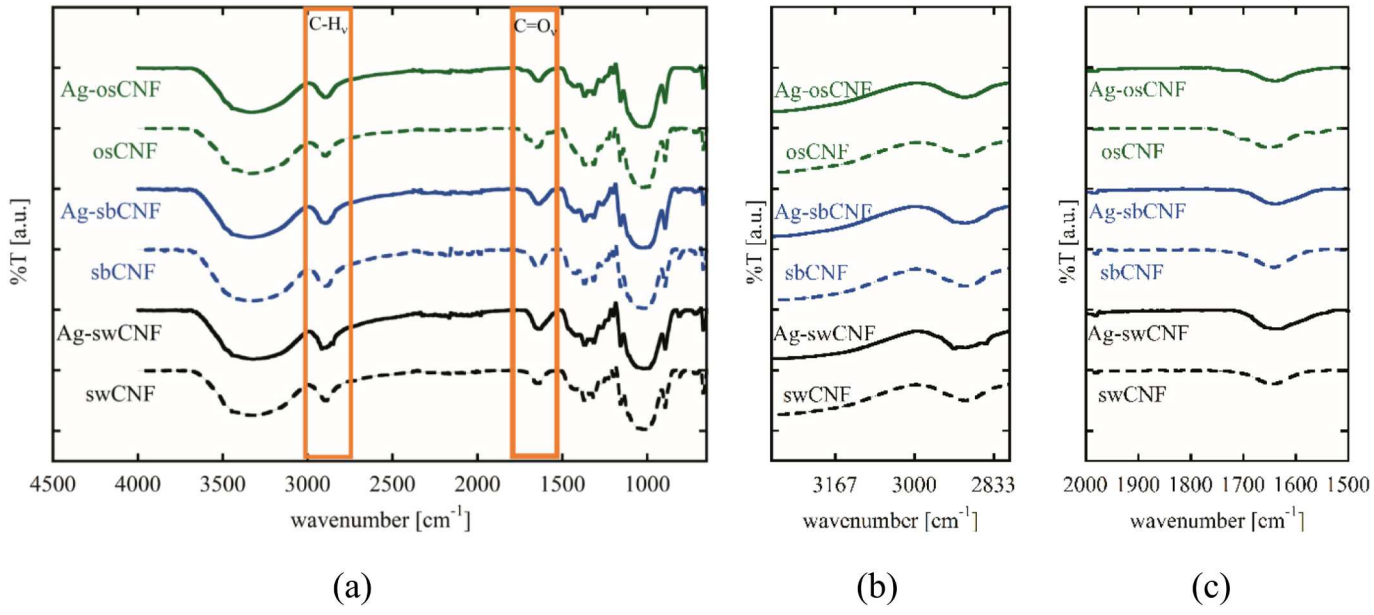

Fig. 3. FTIR-ATR spectra of (a) the beads before and after AgNP formation. (b) magnified images of aldehyde region and (c) carboxyl region.

on the beads was expected and results, making the identification of AgNPs peaks rather challenging. However, a wide peak at 39° is clearly observed, which is attributed to AgNPs and not to adsorbed silver ions (Yang et al., 2016). Most notably, is the clear increase of signal observed in the peaks at 12.4° corresponding to cellulose II allomorph. This may be cause by changes in the crystalline structure of cellulose after interactions with AgNPs, as previously described in the literature (Garcia et al., 2021).

The peak observed at 27° can be observed in a lower degree in cellulose II spectra (Malgas et al., 2020; Nomura et al., 2020), and do not seem to be a result of residual silver nitrate (Aziz et al., 2017). In some hemicellulose, like arabinogalactan, a peak at 27° is also present (Wibowo & Park, 2022). As the osCNF and swCNF hydrogel beads had the highest presence of these other biopolymers, the increased intensity of this peak after the interaction with silver could suggest changes in the accommodation of the hemicelluloses on the surface, affecting the crystallinity.

The quantification of silver content in the different nanocellulose hydrogel beads was done using ICP-EOS (Table 2). These measurements enabled testing of the study's second hypothesis that higher initial surface charge would increase the reducing capacity, generating more AgNPs on the regenerated hydrogel beads. The swCNF hydrogel beads showed the highest amount of silver content with 0.192 mg/L (from the 5 mg/mL hydrolyzed sample), followed by osCNF with 0.172 mg/L and sbCNF with 0.054 mg/L. This trend matched the ash content measured in the TGA and visual observations of brown coloration in the samples. It is worth noting that, as expected, no silver was detected in any of the unmodified nanocellulose hydrogel beads, indicating that the silver content was specifically due to the reduction of silver ions on the surface of the CNFs and not from possible impurities on the water or nitric acid used.

The thermogravimetric analysis (Fig. 5) of the cellulose hydrogel beads showed that there is almost no difference between the hydrogel beads made from swCNF and sbCNF. Conversely, the hydrogel beads made with osCNF had a lower degradation temperature and a mass loss after 450 °C that was reported in the original work due to the residual lignin present in the material (Espinosa et al., 2017). Lower thermal stability has been linked to lower degree of polymerization and higher aldehyde content (Agustin et al., 2016). Which could be possible as agricultural plants had traditionally lower DP than wood fibers (Hallac & Ragauskas, 2011). Another possible factor affecting is that, as the swCNF and sbCNF have lower hydrodynamic radius and higher zeta potential, they dissolved better in the NaOH/urea, increasing the cellulose II content which also increases the thermal stability of the materials (Wei et al., 2020). Furthermore, all unreacted CNFs reached close to 0 % ash content at the end of the TGA experiments.

Once the silver nanoparticles were grown on the fiber surfaces of nanocellulose hydrogel beads, the onset temperature increased for all the materials. However, the full degradation of the cellulose, that normally appears after 400 °C (Wei et al., 2020), presented earlier with the AgNPs as they can help conduct heat and catalyze the degradation (Sivaranjana et al., 2017). As the ash content can be linked to the silver content (Yan et al., 2016), it was of interest to note that the swCNF beads left behind 12 % ash residue, followed by the osCNF beads with 3 %, and the sbCNF beads with 2.3 %.

The morphological appearance of the formed nanocellulose hydrogel beads were observed through SEM images (Fig. 6). These revealed that all the hydrogel beads presented macro and microporosity, with not a visible change before and after AgNP formation, confirming that the process did not break the supra-structure. Evident fiber formation with the regeneration process can be seen on the walls of the pores, especially visible for the osCNF and Ag-osCNF (Fig. 6e and f). The sbCNF, both with and without AgNP (Fig. 6c and d) had a thicker external wall, which may be attributed to the fibers size and low polydispersity in the hydrodynamic radius, affecting the cellulose regeneration (Gericke et al., 2013). At the obtainable scale in these images, the presence of the nanoparticles cannot be assessed.

A better comparison of the morphological differences was obtained with the measurement of the surface energy and area, seeing the changes in functional groups and energy profiles that could occur after nanocellulose dissolution and regeneration. Table 2 presents the dispersive surface energy (γd), acid-base surface energy (γab), and total surface energy (γt = γd + γab), as well as the hydrophilicity index (γab/γt) and the specific surface area (SSA) of the samples as measured by iCG.

The results of surface energy of the unmodified nanocellulose hydrogel beads followed a similar trend to the charge density, with swCNF having the highest surface energy values and osCNF having the lowest. The hydrophilicity index of the materials was similar, with all samples presenting values of 0.13–0.14. The SSA of the swCNF and sbCNF hydrogel beads had the same value despite having a significant difference in hydrodynamic radius prior to regeneration, and the osCNF hydrogel beads had 20 % less surface area.

After silver reduction, osCNF hydrogel beads presented the highest surface energy, followed by the swCNF. In contrast, sbCNF presented almost no change in surface energy, consistent with the lower silver content measured in the ICP. For the SSA, the swCNF hydrogel beads increased more than double, followed by osCNF with an increase of about 10 %, and sbCNF presenting no change. This suggests a relationship between the silver content and the surface area increase, indicating that the silver nanoparticles may have helped open the fibrils network when nucleating around them and increasing the porosity.

Overall, these results confirmed the first hypothesis, demonstrating an impact of source material after the regeneration process on properties such as surface area and surface energy of the resulting hydrogel beads. Contrary, these findings negate the second hypothesis, as there is no direct trend between the silver content with carboxyl content nor with the zeta potential measured values.

Yet, the silver nanoparticles were formed on the nanocellulose hydrogel beads and differences were measured with the different source material. The closest relationship that can be deduced from these data is with the particle size polydispersity of the CNFs before dissolution. As sbCNF had the lowest variance and the lower silver content while swCNF had the highest values. The presence of other non-reducing moieties in the CNFs could also influence the silver formation, as not all carboxyl groups on the CNF surface may be available for silver ion reduction after regeneration in the acid baths.

Table 2
Silver content measured by IOC-EOS, Median (50 % percentile of surface energy) of dispersive surface energy (γd), acid-base surface energy (γab), total surface energy (γt = γd + γab), hydrophilicity index (γab/γt), and specific surface area of samples.

	Ag content (mg/L)	γ_d (mJ/m^2)	γ_{ab} (mJ/m^2)	γ_t (mJ/m^2)	γ_{ab}/γ_t	SSA (m^2/g)
swCNF	ND	57.79	9.28	67.09	0.14	1.87 ± 0.03
Ag-swCNF	0.192	65.63	10.87	76.02	0.14	3.84 ± 0.04
sbCNF	ND	56.89	8.85	65.74	0.13	1.87 ± 0.04
Ag-sbCNF	0.054	59.37	8.61	68.09	0.13	1.87 ± 0.01
osCNF	ND	48.70	7.05	55.37	0.13	1.51 ± 0.08
Ag-osCNF	0.172	67.33	12.62	79.95	0.16	1.65 ± 0.16

ND = non detected.

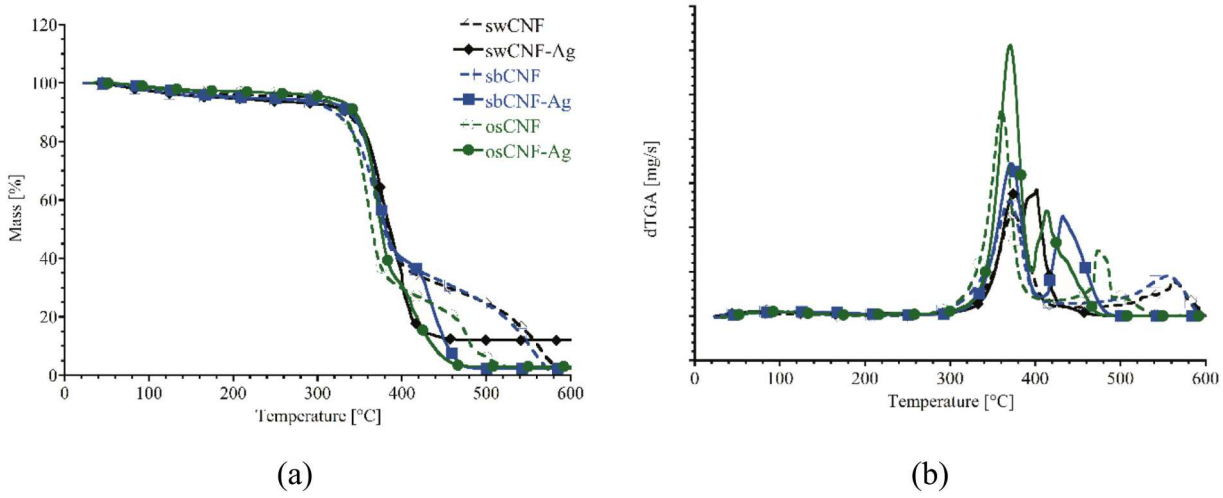

Fig. 5. Thermogravimetric analysis of the beads prior and after silver nanoparticles formation. In (a) the mass loss data is presented, while (b) shows the first derivative.

3.3. Antimicrobial testing

The last hypothesis was that a higher amount of silver would increase the antimicrobial capacity of the nanocellulose hydrogel beads in water samples containing *E. coli*. This was evaluated by the log growth reduction of plated bacteria after passing through syringes packed with different volumes of nanocellulose hydrogel beads. The obtained results are presented in Fig. 7 and the significant value tables of the statistical test are shown in the Supplementary Information.

Overall, the presence of the silver nanoparticles was statistically significant. When the interaction with the materials was done, the significance was maintained for the sbCNF hydrogel beads and the swCNF hydrogel beads but not for the osCNF as in many of the conditions they do not have a significant difference.

At the lowest concentrations (0–2 CFU) there were less instances where significance was found; with sbCNF hydrogel beads eliminating the bacteria even at low material concentrations (13 mm). At the highest contact time (39 mm), swCNF hydrogel beads also had a significant reduction of the bacteria. This variability could be expected as higher error was most plausible at being a yes/no presence test.

At medium concentrations (5–20 CFU/mL), trends started to be visible. The sbCNF-based hydrogel beads were also the best performing and significantly outperformed the osCNF and swCNF hydrogel beads at all filter heights. Here, the effect of the presence of the silver nanoparticles was best seen at the 2 s contact time (26 mm), as all the source materials were significantly different, but the non-AgNP containing osCNF were better than the Ag-osCNF.

At higher concentrations (200–600 CFU), the Ag-sbCNF beads were significantly different at all filter height, even being able to reduce almost in their totality bacterial growth (log reduction of 1.6) with only 1 s of contact. The clearest summary of the materials capacity can be found at 39 mm filter height. There the silver containing sbCNF and swCNF hydrogel beads were significantly different than their silver-free counterpart. All source materials were significantly different between them with sbCNF being the one that performed the best with a 2-log reduction (100 %).

The results and trends measured in this setup negate the working hypothesis as the antibacterial capacity of nanocellulose hydrogel beads did not follow a linear relationship to the amount of silver in each hydrogel bead. The sbCNF had the lowest silver content but showed the highest potential for inhibiting bacterial growth, while the swCNF had the highest silver content but was ranked as the second-best system for bacterial remotion. The most significant relationship was found between the total surface energy (γ_t in Table 2) of the nanocellulose hydrogel beads and bacterial growth reduction. The hydrogel beads with more hydrophobic surfaces (lowest hydrophilicity index and lower surface energy) induced a more prominent reduction in bacterial detection. This could be attributed to the higher attraction that bacterial surface proteins present with low-energy surfaces. This attraction is reversible as the bacteria would have relatively low adhesion, allowing for maximized silver-bacteria contact while enabling the free passage of bacteria through the filter (Song et al., 2020) or having a sorption effect, retaining the bacteria in the column. Future work, like running the bacteria suspension for longer timeframes, could help clearly identify the main phenomena occurring.

It is also possible that a comparable phenomenon is occurring with the Ag-swCNF beads, which showed a higher density packing that permitted more material with high surface area to be placed in the filter. This would enable relatively slower pass of the bacteria solution, increasing retention times and permitting the interaction of the bacteria with the silver nanoparticle regardless of higher surface energy of this system compared to the sbCNF hydrogel beads (Abebe et al., 2015). Thus, these findings indicate that the Ag-sbCNF hydrogel beads could possess the greatest capacity to inhibit bacterial growth or induce sorption, followed by the Ag-swCNF and Ag-osCNF hydrogel beads, which could be better suited for other applications with higher contact times.

4. Discussion

4.1. Silver nanoparticle formation

Despite severe controversy, the use of silver nanoparticles as antimicrobial agents is still commonly studied due to its effectiveness against a wide variety of microorganisms, from *E. coli* to other coliforms and gram-positive pathogens (Guzman et al., 2012). The research community and regulatory bodies have some reservations on the use of this agent for its possible ecotoxicity and non-specific action mechanisms that could lead to cytotoxicity in humans and other fauna. However, testing in multiple cell lines has shown that no adverse effect at low concentrations exist (Xu et al., 2018). This is of relevance when strategies for its use limits to the delivery of Ag ions and avoids the liberation of the full silver nanoparticles (Vishwanath & Negi, 2021), emphasizing the alignment of the methodology here presented with these safety considerations.

Moreover, this work demonstrates that local production of nanocellulose hydrogel beads can be achieved by using different natural sources, including wood and agri-residues. Likewise, these hydrogel

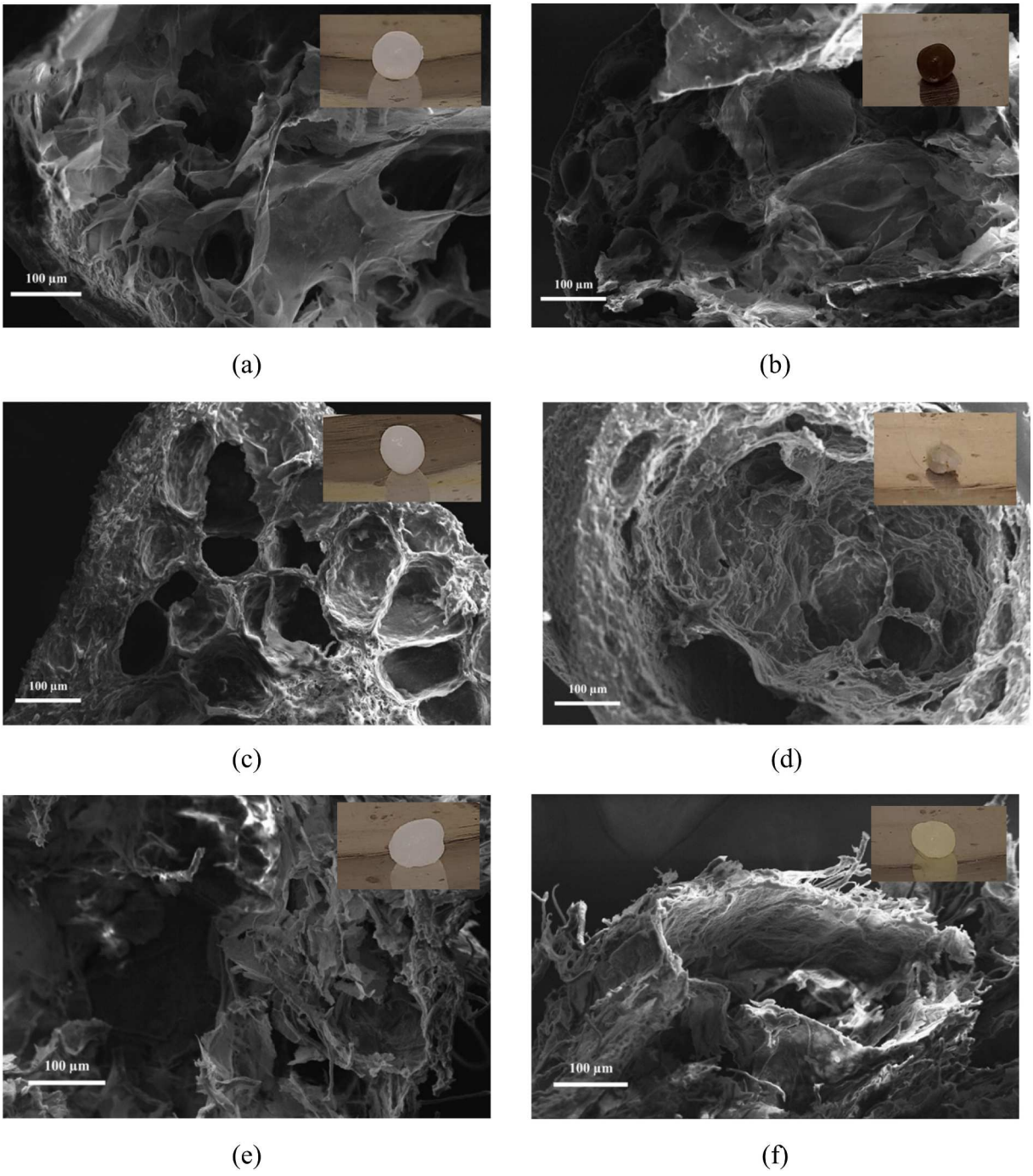

Fig. 6. Scanning electron microscopy images of cryofracture nanocellulose hydrogel beads and insert showing a picture of (a) swCNF, (b) Ag-swCNF, (c) sbCNF, (d) Ag-sbCNF, (e) osCNF; and (f) Ag-osCNF.

beads have demonstrated to be stable under different pH conditions (Gomez-Maldonado, Ponce, & Peresin, 2022). That and the inherent solvent resistance of cellulose give the flexibility to use other green process to seed and grow silver nanoparticle on the hydrogel beads, even using reducing agents like plant and animal isolates (Vishwanath & Negi, 2021). These two factors are of relevance as the need for effective and affordable water filtration systems are more prevalent in rural and developing areas.

Using cellulose as scaffolding for the silver nanoparticles also allows for an ecofriendly and biodegradable approach for antimicrobial filtration systems (Wu et al., 2012; Xu et al., 2018). As demonstrated herein, cellulose can be used not only as substrate (Stinson-Bagby et al., 2019) but also as a reduction agent, tuning the AgNPs content by controlling the starting CNFs particle size and polydispersity. Another method to tune silver content is by controlling the initial silver ions diluted to be reduced in the surface (Wu et al., 2014). While this was not explored in this work, using different initial concentrations has also been studied in other regenerated cellulose microspheres prepared using HCl acid as regeneration media (Wu et al., 2012). Wu's group modulated the silver content on their microspheres to concentrations between 1.1 and 4.9 wt %, like the range of the content measured in this work by ash content in the TGA analysis and ICP.

The use of other reducing agents besides Tollen's reagent such as the traditional $NaBH_4$ (Yan et al., 2016) could also help promote a more

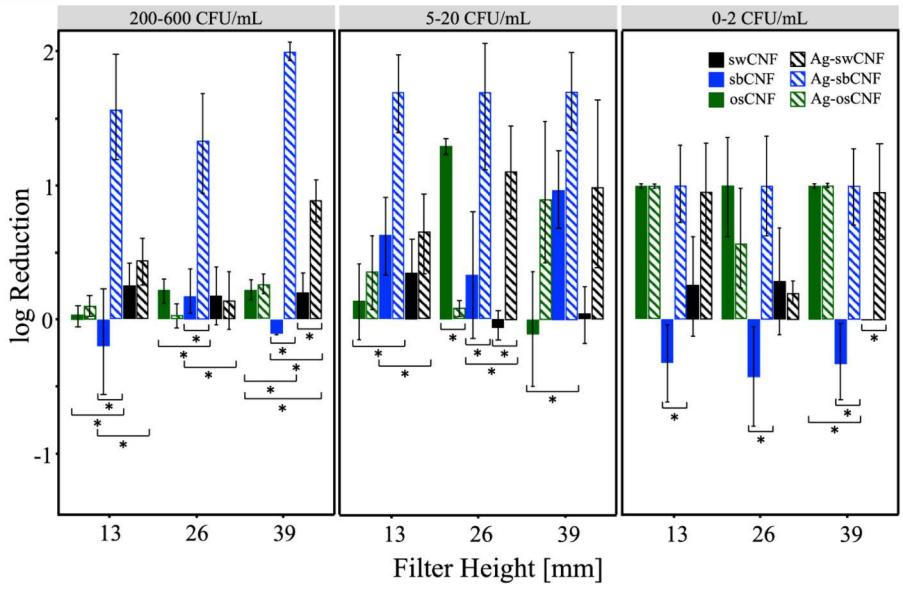

Fig. 7. Log reduction of bacterial growth of solutions with increasing CFU/mL using the hydrogel beads generated with different source materials, used for silver nanoparticle reduction and support, and with different retention times (determined by the filter height). When no CFUs were found, a value of 1 was used to obtain $\log_{10}(1) = 0$. The symbol "*" mark the parings that were significantly different based on multiparametric ANOVA with Tukey test.

direct relationship between the surface groups and the silver content. In the reaction scheme explored herein, silver-ammonia complex facilitates the oxidation of surface hydroxy groups to aldehyde and carboxyl groups that serve as seeding points (Wu et al., 2014). Thus, it coheres that the surface availability (SSA) of cellulose regenerated fibers in the hydrogels, which related to the initial particle size, was the most important factor influencing silver nanoparticle content. As mentioned, this reaction scheme was selected as slow ion release was demonstrated (Wu et al., 2014), lowering the risk of possible collateral toxicity. However, other chemical pathways that use the existing surface moieties might yield different results, demonstrating a more direct impact of the initial surface charge.

4.2. Bacterial removal

As discussed, the most important mechanism of action of the silver nanoparticle comes from the liberation of the ions to the solution in which the bacteria and pathogens are present (Guzman et al., 2012). However, Le Ouay and Stellacci (2015) described the antimicrobial activity of the silver nanoparticles as a more complex system that also involve cell-nanoparticle surface interactions, which are guided by the zeta potential and stabilizing agents of the nanoparticle. Moreover, the shape of the silver nanoparticles was also demonstrated to have an effect in their antimicrobial efficiency and cytotoxicity (Tang & Zheng, 2018). The nanoparticles generated herein were tightly formed around fibers that have one or two order of magnitude higher than the expected AgNPs size (10–30 nm) (Wu et al., 2014). This would have interfered with the surface contact of bacteria and the AgNPs within the one to three seconds flow path in the packed filter. These short or null contact times possibly explain why there was not a proportional relationship between silver content and bacterial growth reduction.

Likely, the most relevant factor driving the bacterial removal after interactions with the materials studied in this work was their surface energy. As noted, sbCNF showed the lowest surface energy and higher bacterial growth reduction. Hydrophobicity on filtration systems have been linked to enhanced interactions between bacteria and antimicrobial agents such as the silver nanoparticles (Ghosh et al., 2019; Song et al., 2020). Similarly, interactions between CNMs and other systems such as small molecules have been shown to be linked to a entropic driven behavior in the hydrophobic face of the structures (Lombardo & Thielemans, 2019). As demonstrated in this work, the formation of the cellulose hydrogel beads with different source materials yielded different surface energies and hydrophobic factors, with the sbCNF presenting the lowest surface energy. This suggests that the hydrophobicity in cellulose-based antibacterial systems should be considered in the design of new applications, independently of the addition of silver nanoparticles.

Other research in archived literature suggest that hydrophilic materials tend to interact with bacteria best due to the higher retention times (Rabiei et al., 2023; Xu et al., 2018). Although this contrasts with the findings herein, the well-known amphipathic behavior of cellulose (Iglesias et al., 2023), and hydrophilicity of the resulting hydrogel beads, presents the opportunity to develop more mechanistic studies to develop a better understanding of the surface phenomena responsible for the bacterial removal of cellulose-silver nanoparticle composites. The limited contact time of the antimicrobial tests presented in this work demonstrated the importance of the hydrophobic phenomena in bacterial removal. Other conclusive indications of important phenomena are limited in this work, factors like the diffusion of silver ions in the hydrogel, especially when contact times can be considered infinite in the bacteria lifetime, should also be considered in future experimental designs.

The versatility of the process presented in this work using cold alkaline dissolution of cellulose nanofibrils suspensions and subsequent reshaping in acidic media, allows for the formation of other shapes of interest such as membranes, fibers, or even 3D printed structures. These new shapes could be used to maximize contact times between the bacteria and silver ions, permitting a deeper understanding of the complex antimicrobial phenomena. Hence, the generated silver containing hydrogels from this study demonstrated bacterial remotion capacity and provided insight into other mechanistic factors like direct contact by the entropic driven interaction between the silver containing cellulose scaffold and the bacteria.

5. Conclusions

Overall, this work presents a sustainable antimicrobial system that could be locally sourced and produced to be used for water filtration. Herein, different source materials were compared, including wood and agri-residues, for the formation of nanocellulose hydrogel beads that

were then used as scaffolds for silver nanoparticles growth and *E. coli* elimination. The methods selected here for nanocellulose hydrogel beads production and silver nanoparticle synthesis demonstrated that considerations like initial surface availability were the most important factor in this system. While surface energy and hydrophobicity were the main drivers in bacterial removal in the packing systems used herein, where ion diffusion time was limited, thus relying on surface contact for the inactivation or sorption of *E. coli*. Alternative approaches to the synthesis method with plant and animal isolates as reducing agents might be beneficial to study in further systems as well as more systematic studies of surface charge, porosity, and bead size when contact times are extended to develop a deeper understanding of the mechanism driving antimicrobial activity on cellulose-silver nanoparticles composites. Future work incorporating dynamic flow simulation tools, considering osmotic pressures and diffusion rates, as well as live/dead fluorescent staining assays may also provide a better understanding of the impact of each condition on the antibacterial properties of the proposed packed column system.

Abbreviations

CNFs	cellulose nanofibrils
CNMs	cellulose nanomaterials
Ag	silver
AgNP	silver nanoparticles
Ag-CNFs	silver-functionalized hydrogel beads
swCNF	bleached softwood cellulose nanofibrils
sbCNF	soybean hull cellulose nanofibrils
osCNF	bleached oat straw nanofibrils
pDADMAC	polydiallyldimethylammonium chloride
PVSK	potassium polyvinyl sulfate
PBS	phosphate buffer saline
LB	Luria broth
OD	optical density
DLS	dynamic light scattering
FTIR-ATR	Fourier transformed infrared spectroscopy with attenuated total reflectance
XRD	X-ray diffraction
TGA	thermogravimetric analysis
SEM	scanning electron microscopy
iGC	inverse gas chromatography
ICP-OES	Inductively coupled plasma with optical emission spectrometry
EPA	Environmental Protection Agency
CFU	colony forming units
ANOVA	analysis of variance
AFM	atomic force microscopy
γd	dispersive surface energy
γab	acid-base surface energy
γt	total surface energy
SSA	specific surface area

Funding sources

This work was supported by the National Science Foundation CAREER award (2119809) through the BMAT program in the Division of Materials Research and the EPSCoR program. Likewise, the USDA National Institute of Food and Agriculture, Hatch program (ALA013-17003), and McIntire-Stennis program (1022526) are thanked for the support of this work.

CRediT authorship contribution statement

Diego Gomez-Maldonado: Writing – original draft, Visualization, Supervision, Methodology, Investigation, Formal analysis, Data curation, Conceptualization. **Brieanne R. Dickson:** Visualization, Investigation, Formal analysis. **Gabriel Au:** Writing – review & editing, Methodology, Investigation, Formal analysis. **Michael J. Bortner:** Validation, Resources, Investigation, Formal analysis. **Mi Li:** Writing – review & editing, Resources, Investigation, Formal analysis, Data curation. **Eduardo Espinosa:** Writing – review & editing, Resources. **Alejandro Rodriguez:** Writing – review & editing, Resources, Conceptualization. **Brendan Higgins:** Writing – review & editing, Validation, Supervision, Resources, Methodology, Conceptualization. **Maria S. Peresin:** Writing – review & editing, Visualization, Supervision, Resources, Project administration, Funding acquisition, Formal analysis, Conceptualization.

Declaration of competing interest

The authors declare the following financial interests/personal relationships which may be considered as potential competing interests: Maria S. Peresin reports financial support was provided by National Science Foundation. Maria S. Peresin reports financial support was provided by National Institute of Food and Agriculture. If there are other authors, they declare that they have no known competing financial interests or personal relationships that could have appeared to influence the work reported in this paper.

Data availability

The data that support the findings of this study are available from the corresponding author upon reasonable request.

Acknowledgements

The authors want to acknowledge Tina Ciaramitaro for her help collecting SEM images and beads manufacturing. The help of Sebastian Gomez-Maldonado for setting up the R code for the multifactor ANOVA test is also highly appreciated. The authors want to acknowledge the Virginia Tech Soil Testing Lab, Ethan Frederick, and Yimin Yao for their help in the ICP-EOS testing; and Sydney Brake and Duber E. Garces Martinez for their help to perform the XRD measurements.

Appendix A. Supplementary data

Supplementary data to this article can be found online at https://doi.org/10.1016/j.carbpol.2024.122771.

References

Abebe, L. S., Su, Y. H., Guerrant, R. L., Swami, N. S., & Smith, J. A. (2015). Point-of-use removal of Cryptosporidium parvum from water: Independent effects of disinfection by silver nanoparticles and silver ions and by physical filtration in ceramic porous media. *Environmental Science and Technology, 49*(21), 12958–12967. https://doi.org/10.1021/acs.est.5b02183

Agustin, M. B., Nakatsubo, F., & Yano, H. (2016). The thermal stability of nanocellulose and its acetates with different degree of polymerization. *Cellulose, 23*(1), 451–464. https://doi.org/10.1007/s10570-015-0813-x

Aziz, S. B., Abdulwahid, R. T., Rasheed, M. A., Abdullah, O. G. H., & Ahmed, H. M. (2017). Polymer blending as a novel approach for tuning the SPR peaks of silver nanoparticles. *Polymers, 9*(10), 486. https://doi.org/10.3390/polym9100486

Barth, S. A., Blome, S., Cornelis, D., Pietschmann, J., Laval, M., Maestrini, O., … Jori, F. (2018). Faecal Escherichia coli as biological indicator of spatial interaction between domestic pigs and wild boar (Sus scrofa) in Corsica. *Transboundary and Emerging Diseases, 65*(3), 746–757. https://doi.org/10.1111/tbed.12799

Bolds, S. A., Lockaby, B. G., Ditchkoff, S. S., Smith, M. D., & VerCauteren, K. C. (2021). Impacts of a large invasive mammal on water quality in riparian ecosystems. *Journal of Environmental Quality, 50*(2), 441–453. https://doi.org/10.1002/jeq2.20194

Bolds, S. A., Lockaby, B. G., Kalin, L., Ditchkoff, S. S., Smith, M. D., & VerCauteren, K. C. (2022). Wild pig removal reduces pathogenic bacteria in low-order streams. *Biological Invasions, 24*(5), 1453–1463. https://doi.org/10.1007/s10530-022-02731-8

Carpenter, A. W., de Lannoy, C.-F., & Wiesner, M. R. (2015). Cellulose nanomaterials in water treatment technologies. *Environmental Science & Technology, 49*(9), 5277–5287. https://doi.org/10.1021/es506351r

De Silva, R., & Byrne, N. (2017). Utilization of cotton waste for regenerated cellulose fibres: Influence of degree of polymerization on mechanical properties. *Carbohydrate Polymers, 174*, 89–94. https://doi.org/10.1016/j.carbpol.2017.06.042

Drogat, N., Granet, R., Sol, V., Memmi, A., Saad, N., Klein Koerkamp, C., Bressollier, P., & Krausz, P. (2011). Antimicrobial silver nanoparticles generated on cellulose nanocrystals. *Journal of Nanoparticle Research, 13*(4), 1557–1562. https://doi.org/10.1007/s11051-010-9995-1

Espinosa, E., Sánchez, R., Otero, R., Domínguez-Robles, J., & Rodríguez, A. (2017). A comparative study of the suitability of different cereal straws for lignocellulose nanofibers isolation. *International Journal of Biological Macromolecules, 103*, 990–999. https://doi.org/10.1016/j.ijbiomac.2017.05.156

Espinosa, E., Tarrés, Q., Delgado-Aguilar, M., González, I., Mutjé, P., & Rodríguez, A. (2016). Suitability of wheat straw semichemical pulp for the fabrication of lignocellulosic nanofibres and their application to papermaking slurries. *Cellulose, 23*(1), 837–852. https://doi.org/10.1007/s10570-015-0807-8

Fan, M., Dai, D., & Huang, B. (2012). Fourier transform infrared spectroscopy for natural Fibres. *Fourier Transform-Materials Analysis.*. https://doi.org/10.5772/35482

Feng, J., Shi, Q., Li, W., Shu, X., Chen, A., Xie, X., & Huang, X. (2014). Antimicrobial activity of silver nanoparticles in situ growth on TEMPO-mediated oxidized bacterial cellulose. *Cellulose, 21*(6), 4557–4567. https://doi.org/10.1007/s10570-014-0449-2

Fiorati, A., Bellingeri, A., Punta, C., Corsi, I., & Venditti, I. (2020). Silver nanoparticles for water pollution monitoring and treatments: Ecosafety challenge and cellulose-based hybrids solution. *Polymers, 12*(8), 1635. https://doi.org/10.3390/polym12081635

Foster, E. J., Moon, R. J., Agarwal, U. P., Bortner, M. J., Bras, J., Camarero-Espinosa, S., … Youngblood, J. (2018). Current characterization methods for cellulose nanomaterials. In *Chemical society reviews* (pp. 2609–2679). https://doi.org/10.1039/c6cs00895j

Garcia, A. M., Martins, T. S., & Camilo, F. F. (2021). Free facile preparation of Ag-nanoparticles on cellulose membrane for catalysis. *Cellulose, 28*(8), 4899–4911. https://doi.org/10.1007/s10570-021-03827-5

Gericke, M., Trygg, J., & Fardim, P. (2013). Functional cellulose beads: Preparation, characterization, and applications. *Chemical Reviews, 113*(7), 4812–4836. https://doi.org/10.1021/cr300242j

Ghosh, S., Das, P., Ganguly, S., Remanan, S., Das, T. K., Bhattacharyya, S. K., … Das, N. C. (2019). 3D-enhanced, high-performing, super-hydrophobic and electromagnetic-interference shielding fabrics based on silver paint and their use in antibacterial applications. *ChemistrySelect, 4*(40), 11748–11754. https://doi.org/10.1002/slct.201901738

Gomez-Maldonado, D., Ponce, S., & Peresin, M. S. (2022). The applicability of cellulose — Tara gum composite hydrogels as dye capture adsorbents. *Water, Air, & Soil Pollution, 1–13*. https://doi.org/10.1007/s11270-022-05818-z

Gomez-Maldonado, D., Reynolds, A. M., Burnett, D. J., Babu, R. J., Waters, M. N., & Peresin, M. S. (2022). Delignified wood aerogels as scaffolds coated with an oriented chitosan–cyclodextrin co-polymer for removal of microcystin-LR. *RSC Advances, 12*(31), 20330–20339. https://doi.org/10.1039/D2RA03556A

Gomez-Maldonado, D., Reynolds, A. M., Johansson, L.-S., Burnett, D. J., Ramapuram, J. B., Waters, M. N., … Peresin, M. S. (2021). Fabrication of aerogels from cellulose nanofibril grafted with β-cyclodextrin for capture of water pollutants. *Journal of Porous Materials, 28*(6), 1725–1736. https://doi.org/10.1007/s10934-021-01109-w

Guzman, M., Dille, J., & Godet, S. (2012). Synthesis and antibacterial activity of silver nanoparticles against gram-positive and gram-negative bacteria. *Nanomedicine: Nanotechnology, Biology, and Medicine, 8*(1), 37–45. https://doi.org/10.1016/j.nano.2011.05.007

Hallac, B. B., & Ragauskas, A. J. (2011). Analyzing cellulose degree of polymerization and its relevancy to cellulosic ethanol. *Biofuels, Bioproducts and Biorefining, 5*(2), 215–225. https://doi.org/10.1002/bbb.269

Hernandez, J. A., Soni, B., Iglesias, M. C., Vega Erramuspe, I. B., Frazier, C. E., & Peresin, M. S. (2022). Soybean hull pectin and nanocellulose: Tack properties in aqueous pMDI dispersions. *Journal of Materials Science, 57*(8), 5022–5035. https://doi.org/10.1007/s10853-022-06938-x

Iglesias, M. C., Gomez-Maldonado, D., Davis, V. A., & Peresin, M. S. (2023). A review on lignocellulose chemistry, nanostructure, and their impact on interfacial interactions for sustainable products development. *Journal of Materials Science, 58*(2), 685–706. https://doi.org/10.1007/s10853-022-07992-1

Iglesias, M. C., Gomez-Maldonado, D., Via, B. K., Jiang, Z., & Peresin, M. S. (2020). Pulping processes and their effects on cellulose fibers and nanofibrillated cellulose properties: A review. *Forest Products Journal, 70*(1), 10–21. https://doi.org/10.13073/FPJ-D-19-00038

Iglesias, M. C., Hamade, F., Aksoy, B., Jiang, Z., Davis, V. A., & Peresin, M. S. (2021). Correlations between rheological behavior and intrinsic properties of nanofibrillated cellulose from wood and soybean hulls with varying lignin content. *BioResources, 16*(3), 4831–4845. https://doi.org/10.15376/biores.16.3.4831-4845

Ishii, S., & Sadowsky, M. J. (2008). Escherichia coli in the environment: Implications for water quality and human health. *Microbes and Environments, 23*(2), 101–108. https://doi.org/10.1264/jsme2.23.101

Jiang, Z., Fang, Y., Xiang, J., Ma, Y., Lu, A., Kang, H., Huang, Y., Guo, H., Liu, R., & Zhang, L. (2014). Intermolecular interactions and 3D structure in cellulose-NaOH-urea aqueous system. *Journal of Physical Chemistry B, 118*(34), 10250–10257. https://doi.org/10.1021/jp501408e

Karlsson, R. M. P., Larsson, P. T., Hansson, P., & Wågberg, L. (2019). Thermodynamics of the water-retaining properties of cellulose-based networks. *Biomacromolecules, 20*(4), 1603–1612. https://doi.org/10.1021/acs.biomac.8b01791

Klemm, D., Heublein, B., Fink, H. P., & Bohn, A. (2005). Cellulose: Fascinating biopolymer and sustainable raw material. *Angewandte Chemie, International Edition, 44*(22), 3358–3393. https://doi.org/10.1002/anie.200460587

Le Ouay, B., & Stellacci, F. (2015). Antibacterial activity of silver nanoparticles: A surface science insight. *Nano Today, 10*(3), 339–354. https://doi.org/10.1016/j.nantod.2015.04.002

Liao, C., Li, Y., & Tjong, S. (2019). Bactericidal and cytotoxic properties of silver nanoparticles. *International Journal of Molecular Sciences, 20*(2), 449. https://doi.org/10.3390/ijms20020449

Lin, S., Chen, L., Huang, L., Cao, S., Luo, X., & Liu, K. (2015). Novel antimicrobial chitosan-cellulose composite films bioconjugated with silver nanoparticles. *Industrial Crops and Products, 70*, 395–403. https://doi.org/10.1016/j.indcrop.2015.03.040

Lombardo, S., & Thielemans, W. (2019). Thermodynamics of adsorption on nanocellulose surfaces. *Cellulose, 26*(1), 249–279. https://doi.org/10.1007/s10570-018-02239-2

Małachowska, E., Dubowik, M., Boruszewski, P., Łojewska, J., & Przybysz, P. (2020). Influence of lignin content in cellulose pulp on paper durability. *Scientific Reports, 10*(1). https://doi.org/10.1038/s41598-020-77101-2

Malgas, S., Kwanya Minghe, V. M., & Pletschke, B. I. (2020). The effect of hemicellulose on the binding and activity of cellobiohydrolase I, Cel7A, from Trichoderma reesei to cellulose. *Cellulose, 27*(2), 781–797. https://doi.org/10.1007/s10570-019-02848-5

McDonough, M. T., Ditchkoff, S. S., Smith, M. D., & Vercauteren, K. C. (2022). A review of the impacts of invasive wild pigs on native vertebrates. In *, vol. 102, issue 2. Mammalian biology* (pp. 279–290). Springer Science and Business Media Deutschland GmbH. https://doi.org/10.1007/s42991-022-00234-6.

Nomura, S., Kugo, Y., & Erata, T. (2020). 13C NMR and XRD studies on the enhancement of cellulose II crystallinity with low concentration NaOH post-treatments. *Cellulose, 27*(7), 3553–3563. https://doi.org/10.1007/s10570-020-03036-6

Olivera, S., Muralidhara, H. B., Venkatesh, K., Guna, V. K., Gopalakrishna, K., Kumar, K., & Y.. (2016). Potential applications of cellulose and chitosan nanoparticles/composites in wastewater treatment: A review. *Carbohydrate Polymers, 153*, 600–618. https://doi.org/10.1016/j.carbpol.2016.08.017

Qi, H., Chang, C., & Zhang, L. (2008). Effects of temperature and molecular weight on dissolution of cellulose in NaOH/urea aqueous solution. *Cellulose, 15*(6), 779–787. https://doi.org/10.1007/s10570-008-9230-8

R Core Team. (2023). The R project for statistical computing. https://www.r-project.org.

Rabiei, H., Torshabi, M., Montazer, M., Khaloo, S. S., & Dehghan, S. F. (2023). Antimicrobial activity and cytotoxicity of cotton-polyester fabric coated with a metal–organic framework and metal oxide nanoparticle. *Applied Nanoscience (Switzerland)*.. https://doi.org/10.1007/s13204-023-02823-4

Redlinger-Pohn, J. D., König, J., & Radl, S. (2017). Length-selective separation of cellulose fibres by hydrodynamic fractionation. *Chemical Engineering Research and Design, 126*, 54–66. https://doi.org/10.1016/j.cherd.2017.08.001

Roy, D., Semsarilar, M., Guthrie, J. T., & Perrier, S. (2009). Cellulose modification by polymer grafting: A review. *Chemical Society Reviews, 38*(7), 2046–2064. https://doi.org/10.1039/b808639g

Sivaranjana, P., Nagarajan, E. R., Rajini, N., Jawaid, M., & Rajulu, A. V. (2017). Cellulose nanocomposite films with in situ generated silver nanoparticles using Cassia alata leaf extract as a reducing agent. *International Journal of Biological Macromolecules, 99*, 223–232. https://doi.org/10.1016/j.ijbiomac.2017.02.070

Sokal, R. R., & Rohlf, F. J. (1987). *Introduction to biostatistics*. Dover Publications.

Song, B., Zhang, E., Han, X., Zhu, H., Shi, Y., & Cao, Z. (2020). Engineering and application perspectives on designing an antimicrobial surface. In *, vol. 12, issue 19. ACS applied materials and interfaces* (pp. 21330–21341). American Chemical Society. https://doi.org/10.1021/acsami.9b19992.

Stinson-Bagby, K. L., Owens, J., Rouffa, A., Bortner, M. J., & Foster, E. J. (2019). Silver nanoparticle pulsed synthesis and attachment to cellulose nanocrystals. *ACS Applied Nano Materials, 2*(4), 2317–2324. https://doi.org/10.1021/acsanm.9b00225

Tang, S., & Zheng, J. (2018). Antibacterial activity of silver nanoparticles: Structural effects. In *, Vol. 7, Issue 13. Advanced healthcare materials*. Wiley-VCH Verlag. https://doi.org/10.1002/adhm.201701503.

Trygg, J., & Fardim, P. (2011). Enhancement of cellulose dissolution in water-based solvent via ethanol-hydrochloric acid pretreatment. *Cellulose, 18*(4), 987–994. https://doi.org/10.1007/s10570-011-9550-y

US Environmental Protection Agency. (1996). Method 6010B. *4*(1), 1–25.

Valencia, L., Kumar, S., Nomena, E. M., Salazar-Alvarez, G., & Mathew, A. P. (2020). In-situ growth of metal oxide nanoparticles on cellulose nanofibrils for dye removal and antimicrobial applications. *ACS Applied Nano Materials, 3*(7), 7172–7181. https://doi.org/10.1021/acsanm.0c01511

Vishwanath, R., & Negi, B. (2021). Conventional and green methods of synthesis of silver nanoparticles and their antimicrobial properties. In *, Vol. 4. Current research in green and sustainable chemistry*. Elsevier B.V. https://doi.org/10.1016/j.crgsc.2021.100205.

Wang, S., Lu, A., & Zhang, L. (2016). Recent advances in regenerated cellulose materials. *Progress in Polymer Science, 53*, 169–206. https://doi.org/10.1016/j.progpolymsci.2015.07.003

Wei, Q. Y., Lin, H., Yang, B., Li, L., Zhang, L. Q., Huang, H. D., … Li, Z. M. (2020). Structure and properties of all-cellulose composites prepared by controlling the dissolution temperature of a NaOH/urea solvent. *Industrial and Engineering Chemistry Research, 59*(22), 10428–10435. https://doi.org/10.1021/acs.iecr.9b07075

Wibowo, E. S., & Park, B. D. (2022). Effect of hemicellulose molecular structure on wettability and surface adhesion to urea–formaldehyde resin adhesives. *Wood Science and Technology, 56*(4), 1047–1070. https://doi.org/10.1007/s00226-022-01397-8

Wohlhauser, S., Delepierre, G., Labet, M., Morandi, G., Thielemans, W., Weder, C., & Zoppe, J. O. (2018). Grafting polymers from cellulose nanocrystals: Synthesis,

properties, and applications. *Macromolecules, 51*(16), 6157–6189. https://doi.org/10.1021/acs.macromol.8b00733

Wu, J., Zhao, N., Zhang, X., & Xu, J. (2012). Cellulose/silver nanoparticles composite microspheres: Eco-friendly synthesis and catalytic application. *Cellulose, 19*(4), 1239–1249. https://doi.org/10.1007/s10570-012-9731-3

Wu, J., Zheng, Y., Song, W., Luan, J., Wen, X., Wu, Z., Chen, X., Wang, Q., & Guo, S. (2014). In situ synthesis of silver-nanoparticles/bacterial cellulose composites for slow-released antimicrobial wound dressing. *Carbohydrate Polymers, 102*(1), 762–771. https://doi.org/10.1016/j.carbpol.2013.10.093

Xu, Y., Li, S., Yue, X., & Lu, W. (2018). Review of silver nanoparticles (AgNPs)-cellulose antibacterial composites. *BioResources, 13*(1), 2150–2170.

Yan, J., Abdelgawad, A. M., El-Naggar, M. E., & Rojas, O. J. (2016). Antibacterial activity of silver nanoparticles synthesized in-situ by solution spraying onto cellulose. *Carbohydrate Polymers, 147*, 500–508. https://doi.org/10.1016/j.carbpol.2016.03.029

Yang, H., Ren, Y.y., Wang, T., & Wang, C. (2016). Preparation and antibacterial activities of Ag/Ag+/Ag3+ nanoparticle composites made by pomegranate (Punica granatum) rind extract. *Results in Physics, 6*, 299–304. https://doi.org/10.1016/j.rinp.2016.05.012